RESEARCH ARTICLE SUMMARY

SINGLE-CELL GENOMICS

Developmental cell programs are co-opted in inflammatory skin disease

Gary Reynolds*, Peter Vegh*, James Fletcher*, Elizabeth F. M. Poyner*, Emily Stephenson, Issac Goh, Rachel A. Botting, Ni Huang, Bayanne Olabi, Anna Dubois, David Dixon, Kile Green, Daniel Maunder, Justin Engelbert, Mirjana Efremova, Krzysztof Polański, Laura Jardine, Claire Jones, Thomas Ness, Dave Horsfall, Jim McGrath, Christopher Carey, Dorin-Mirel Popescu, Simone Webb, Xiao-nong Wang, Ben Sayer, Jong-Eun Park, Victor A. Negri, Daria Belokhvostova, Magnus D. Lynch, David McDonald, Andrew Filby, Tzachi Hagai, Kerstin B. Meyer, Akhtar Husain, Jonathan Coxhead, Roser Vento-Tormo, Sam Behjati, Steven Lisgo, Alexandra-Chloé Villani, Jaume Bacardit, Philip H. Jones, Edel A. O'Toole, Graham S. Ogg, Neil Rajan, Nick J. Reynolds, Sarah A. Teichmann†, Fiona M. Watt†, Muzlifah Haniffa†

INTRODUCTION: Human skin provides vital protection from water loss and from external insult through structural adaptations and interplay with the innate and adaptive immune systems. The skin develops and functions in an aquatic environment in utero but rapidly adapts to a contrasting set of physical and pathogenic challenges after birth. The changes that take place across this complex multicellular system during development and upon perturbation by immune-mediated inflammatory diseases are poorly understood. A detailed study will facilitate the development of therapeutic interventions for inflammatory skin disease.

RATIONALE: We generated a comprehensive atlas of human skin in early prenatal life, in adulthood, and during inflammatory skin disease by profiling the transcriptomes of more than 500,000 single cells. We analyzed human embryonic skin between 7 and 10 post-conception weeks, healthy adult skin surplus from mammoplasty surgery, and skin biopsies from patients affected by atopic dermatitis (AD) and psoriasis, two common inflammatory skin diseases. Additionally, we performed single-cell T cell receptor analysis to assess T cell clonality in disease. Validation experiments were conducted at the protein level and used mass cytometry, flow cytometry, and immunostaining in situ of skin biopsies from healthy skin and patients with AD and psoriasis, including a cohort of AD patients before and during treatment with oral methotrexate.

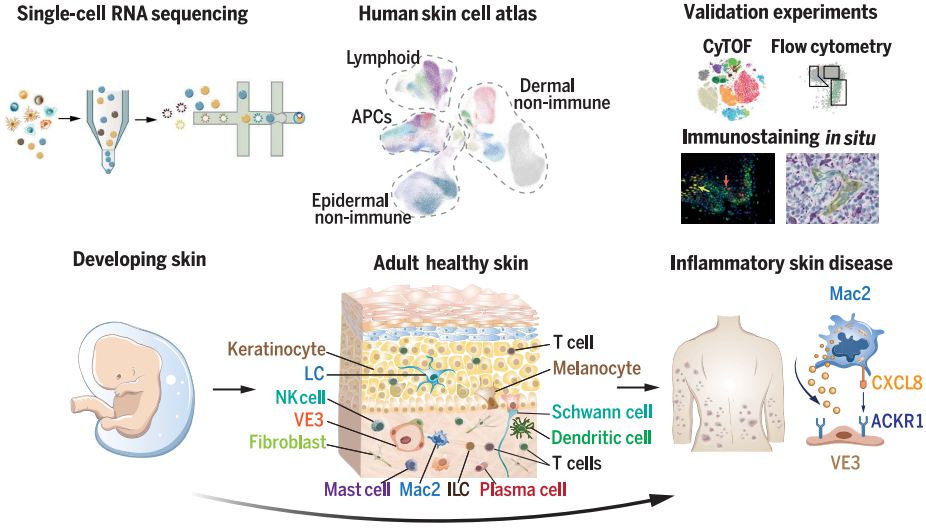

The human skin cell atlas. We used single-cell RNA sequencing to build human skin cell atlases across development, homeostasis, and disease; the analyses were supported by various validation modalities. By delineating cell states in embryonic skin, healthy adult skin, and inflammatory skin diseases (atopic dermatitis and psoriasis), we identified a reemergence of developmental programs in disease mediated by interactions between Mac2 and VE3. APCs, antigen-presenting cells; CyTOF, cytometry by time-of-flight; LC, Langerhans cell; NK, natural killer cell; VE, vascular endothelial cell; Mac, macrophage; ILC, innate lymphoid cell.

RESULTS: Thirty-four cell states were identified in healthy human skin across the collective dataset, with dynamic changes in the nature and abundance of single-cell gene expression profiles identified across embryonic and adult life and upon perturbation during inflammatory skin disease. This resource can be accessed via an interactive browsable web portal, https://developmentcellatlas.ncl.ac.uk/datasets/hca_skin_portal. Analyses revealed that the immune system of first-trimester embryonic skin consists mainly of innate lymphocytes and macrophages. In adult skin, we defined two inferred trajectories for keratinocyte differentiation and the presence of endothelial cells that formed dilated postcapillary venules. We revealed a migratory dendritic cell (DC) signature in healthy adult skin that is conserved in murine DCs. The migratory DC signature was also evident in the developing human thymus and additional disease states. We identified clonally expanded disease-associated cytotoxic T cells (Tc IL13/IL22 cells) in lesional AD and Tc17/T helper 17 (T_H17) cells in lesional psoriasis. We demonstrated the reemergence of prenatal cellular programs mediated by Mac2 macrophages via the chemokine CXCL8 interacting with the venular capillary marker ACKR1 on VE3 vascular endothelial cells in diseased skin. This interaction is implicated in lymphocyte recruitment and angiogenesis. We identified and validated in situ the expansion of Mac2 and VE3 in lesional AD and lesional psoriasis skin, their close apposition in AD and psoriasis tissue, and their reduction in AD skin during methotrexate treatment, which aligned with an improvement in the clinical severity of disease in this patient cohort.

CONCLUSION: Our single-cell atlas of human skin from prenatal life, healthy adults, and AD and psoriasis patients highlights the dynamic nature of cutaneous homeostasis and immunity. Our study provides insights into perturbed and co-opted developmental cellular programs in inflammatory skin disease. These results may provide potential future translational targets to improve the diagnosis and molecular classification of these diseases and to guide treatment strategies. ■

The list of author affiliations is available in the full article online.
*These authors contributed equally to this work.
†Corresponding author. Email: st9@sanger.ac.uk (S.A.T.); fiona.watt@kcl.ac.uk (F.M.W.); m.a.haniffa@newcastle.ac.uk (M.H.)
Cite this article as G. Reynolds *et al.*, *Science* **371**, eaba6500 (2021). DOI: 10.1126/science.aba6500

RESEARCH ARTICLE

SINGLE-CELL GENOMICS

Developmental cell programs are co-opted in inflammatory skin disease

Gary Reynolds[1]*, Peter Vegh[1]*, James Fletcher[1]*, Elizabeth F. M. Poyner[1,2]*, Emily Stephenson[1], Issac Goh[1], Rachel A. Botting[1], Ni Huang[3], Bayanne Olabi[1,4], Anna Dubois[1,2], David Dixon[1], Kile Green[1], Daniel Maunder[1], Justin Engelbert[1], Mirjana Efremova[3], Krzysztof Polański[3], Laura Jardine[1], Claire Jones[1], Thomas Ness[1], Dave Horsfall[1], Jim McGrath[1], Christopher Carey[1], Dorin-Mirel Popescu[1], Simone Webb[1], Xiao-nong Wang[1], Ben Sayer[1], Jong-Eun Park[3], Victor A. Negri[5], Daria Belokhvostova[5], Magnus D. Lynch[5], David McDonald[1], Andrew Filby[1], Tzachi Hagai[6], Kerstin B. Meyer[3], Akhtar Husain[7], Jonathan Coxhead[1], Roser Vento-Tormo[3], Sam Behjati[3,8], Steven Lisgo[1], Alexandra-Chloé Villani[9,10], Jaume Bacardit[11], Philip H. Jones[3,12], Edel A. O'Toole[13], Graham S. Ogg[14], Neil Rajan[1,2], Nick J. Reynolds[2,15], Sarah A. Teichmann[3,16]†, Fiona M. Watt[5]†, Muzlifah Haniffa[1,2,3]†

The skin confers biophysical and immunological protection through a complex cellular network established early in embryonic development. We profiled the transcriptomes of more than 500,000 single cells from developing human fetal skin, healthy adult skin, and adult skin with atopic dermatitis and psoriasis. We leveraged these datasets to compare cell states across development, homeostasis, and disease. Our analysis revealed an enrichment of innate immune cells in skin during the first trimester and clonal expansion of disease-associated lymphocytes in atopic dermatitis and psoriasis. We uncovered and validated in situ a reemergence of prenatal vascular endothelial cell and macrophage cellular programs in atopic dermatitis and psoriasis lesional skin. These data illustrate the dynamism of cutaneous immunity and provide opportunities for targeting pathological developmental programs in inflammatory skin diseases.

Human skin undergoes major adaptations as it transitions from a relatively pathogen-free aquatic environment in utero to provide mechanical and immunological protection in a nonsterile terrestrial environment. This function requires coordination by specialized cell types that are established during embryonic development. The cellular landscape of prenatal and adult skin, however, remains incompletely defined.

In cancer, developmental cell programs such as angiogenesis, proliferation, and invasion reemerge and lead to interaction between malignant cells and the surrounding stroma (*1*–*4*). The current consensus view on inflammatory skin disease pathogenesis is that the interplay between leukocytes and nonleukocytes is involved in disease initiation and progression (*5*). However, it is unknown whether cell states and gene programs observed in prenatal skin contribute to the pathogenesis of adult-onset inflammatory skin disorders. A detailed understanding of this process may provide a new perspective on inflammatory disease pathogenesis and potentially could identify novel therapeutic targets.

Single-cell genomics, such as RNA sequencing, provides an opportunity to dissect the complex cellular organization of human skin during development and in health and disease at a systems level. Studies of healthy skin to date have primarily focused on adult skin, restricted to specific cell lineages and limited cell numbers (*6*–*10*). Large-scale single-cell profiling of human skin should provide a transformative resource to understand aberrations in gene expression resulting from disease.

Deconstructing human skin

In this study, we used single-cell RNA sequencing (scRNA-seq) combined with strategic fluorescence-activated cell sorting (FACS) for comprehensive and deep profiling of healthy and inflamed adult skin. To maximize cell yield and viability from tissue dissociation from previous findings (*11*–*13*), we used 200-μm-thick healthy skin samples resulting from mammoplasty, which were separated into epidermis and dermis before dissociation (Fig. 1A and fig. S1A). We adapted our previous FACS gating strategy (*12*, *14*) to isolate various cell fractions (keratinocytes, fibroblasts, and endothelial cells) and immune cells (myeloid and lymphoid cells) to upsample rare cell types for deep cell sampling. We ensured comprehensive capture, minimizing cell loss by placing these FACS gates contiguously (fig. S1B). FACS-isolated cells were characterized with the 10x Genomics platform. We also performed indexed plate-based Smart-seq2 profiling of all epidermal and dermal cells within the $CD45^{+}HLA\text{-}DR^{+}$ myeloid gate (fig. S1B). To compare cell states in healthy skin with inflammatory disease-induced perturbation, we performed scRNA-seq (10x Genomics) on all $CD45^{-}$ and $CD45^{+}$ cells from lesional and nonlesional skin from patients with atopic dermatitis (AD) and psoriasis (Fig. 1A and fig. S1C).

In total, 528,253 sequenced skin cells (n = 19) passed quality control and doublet exclusion (Fig. 1A). We detected on average ~3000 genes with the 10x Genomics platform and ~6000 genes per cell with Smart-seq2 (*15*) (fig. S2A). We excluded cells with <200 genes, >20% mitochondrial gene expression, and those identified as doublets (*15*). To account for biases due to batch effects, we performed data integration of healthy skin samples using BBKNN implementation within Scanpy (*16*, *17*), which showed good sample mixing by UMAP visualization (Fig. 1B and figs. S1, D and E, and S2B). We performed graph-based Leiden clustering and derived differentially expressed genes to annotate the cell clusters, from which 34 cell states were identified (Fig. 1, B and C, and table S1). We were able to identify these cell states by deconvolution analysis using AutoGeneS (*18*) of adult healthy bulk RNA-seq (fig. S2C). The 34 cell states were discernible even after removal of stress response genes associated with tissue dissociation (*19*) (fig. S2D). We note the impact of different tissue dissociation protocols on gene expression, as previously reported (*20*). We found that the same cell states could be identified in a small dataset using the Miltenyi dissociation protocol (*7*) and through the statistical power and

[1]Biosciences Institute, Newcastle University, Newcastle upon Tyne NE2 4HH, UK. [2]Department of Dermatology and NIHR Newcastle Biomedical Research Centre, Newcastle Hospitals NHS Foundation Trust, Newcastle upon Tyne NE2 4LP, UK. [3]Wellcome Sanger Institute, Wellcome Genome Campus, Hinxton, Cambridge CB10 1SA, UK. [4]Department of Dermatology, NHS Lothian, Lauriston Building, Edinburgh EH3 9EN, UK. [5]Centre for Stem Cells and Regenerative Medicine, King's College London, Guy's Hospital Campus, London SE1 9RT, UK. [6]Shmunis School of Biomedicine and Cancer Research, George S. Wise Faculty of Life Sciences, Tel Aviv University, Tel Aviv 69978, Israel. [7]Department of Pathology, Royal Victoria Infirmary, Newcastle upon Tyne NE1 4LP, UK. [8]Department of Paediatrics, University of Cambridge, Cambridge CB2 0SP, UK. [9]Broad Institute of Harvard and MIT, Cambridge, MA 02142, USA. [10]Center for Immunology and Inflammatory Diseases, Massachusetts General Hospital, Boston, MA 02129, USA. [11]School of Computing, Newcastle University, Newcastle upon Tyne NE4 5TG, UK. [12]MRC Cancer Unit, University of Cambridge, Cambridge CB2 0XZ, UK. [13]Centre for Cell Biology and Cutaneous Research, Blizard Institute, Queen Mary University of London, London, UK. [14]MRC Human Immunology Unit, Oxford Biomedical Research Centre, MRC Weatherall Institute of Molecular Medicine, University of Oxford, Oxford, UK. [15]Translational and Clinical Research Institute, Newcastle University, Newcastle upon Tyne NE2 4HH, UK. [16]Theory of Condensed Matter Group, Cavendish Laboratory/Department of Physics, University of Cambridge, Cambridge CB3 0HE, UK.
*These authors contributed equally to this work.
†Corresponding author. Email: st9@sanger.ac.uk (S.A.T.); fiona.watt@kcl.ac.uk (F.M.W.); m.a.haniffa@newcastle.ac.uk (M.H.)

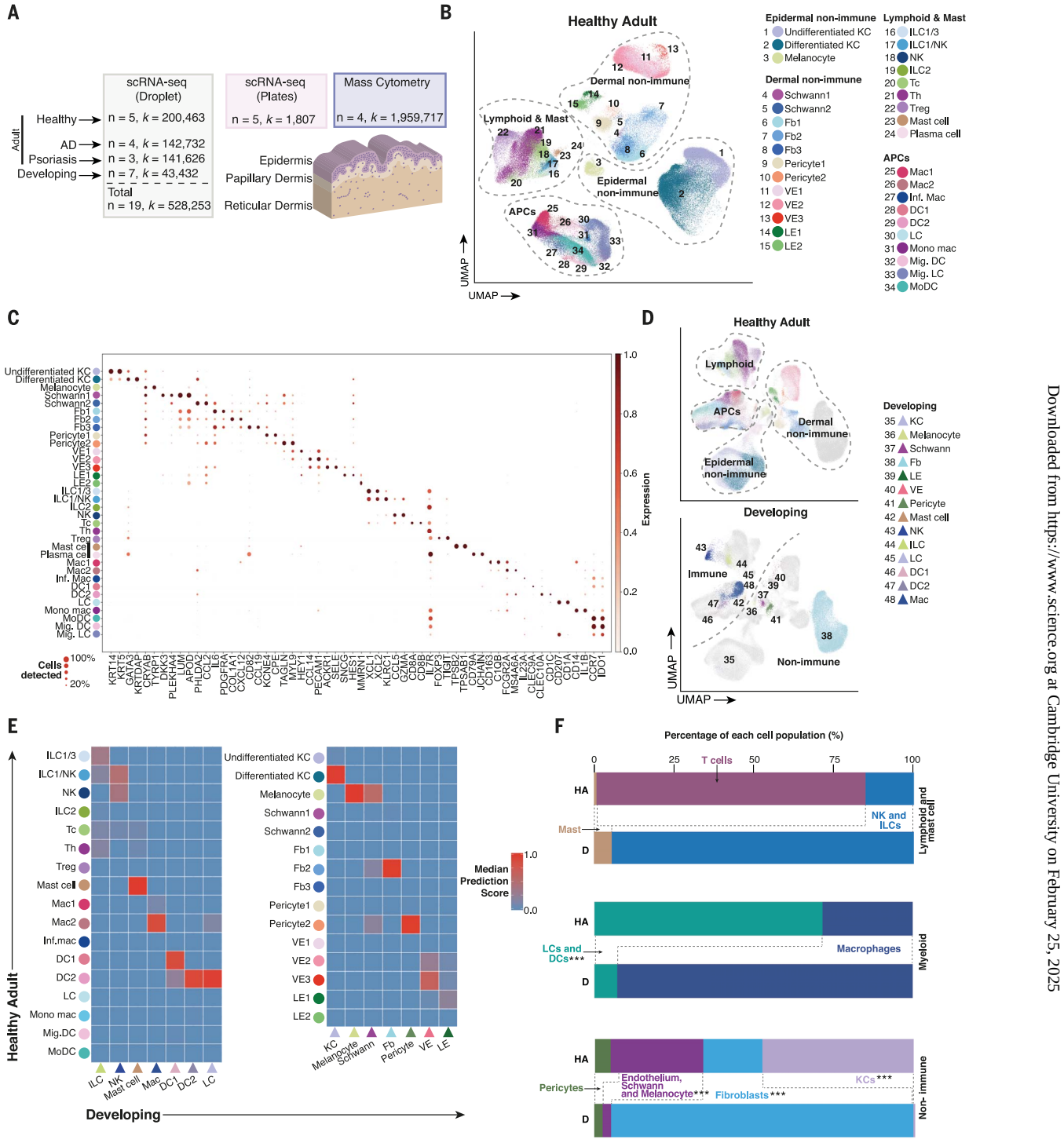

Fig. 1. Deconstructing human skin. (**A**) Numbers of cells profiled by scRNA-seq and mass cytometry for each condition and schematic of sampling locations. AD, atopic dermatitis. (**B**) UMAP visualization showing all cell states found in the healthy adult scRNA-seq dataset (n = 5). KC, keratinocyte; Fb, fibroblast; VE, vascular endothelium; LE, lymphatic endothelium; ILC, innate lymphoid cell; NK, natural killer cell; Tc, cytotoxic T cell; T_H, T helper cell; T_{reg}, regulatory T cell; Mac, macrophage; Inf., inflammatory; DC, dendritic cell; LC, Langerhans cell; Mono mac, monocyte-derived macrophage; Mig., migratory; MoDC, monocyte-derived dendritic cell. (**C**) Dot plot showing the expression of discriminatory markers for each cell state in (B). *CD8A*, *CD163*, *CD14*, and *CCR7* were chosen for CyTOF protein validation. (**D**) Top: UMAP visualization of healthy adult cell states overlaid on developing cell states (n = 7). Bottom: UMAP visualization of developing cell states overlaid on healthy adult cell states. Cells underlaid are shown in gray. (**E**) Median prediction score of developing skin cell states using healthy adult skin as reference derived from the TransferAnchors function in Seurat. Triangles denote developing skin cells; circles denote adult skin cells. (**F**) Bar charts showing the proportions of corresponding cell states found in adult and developing skin. We used generalized linear modeling on a quasi-binomial distribution to compare proportions between developing and adult skin, and found statistically significant changes in vascular endothelium, Schwann cells, and melanocytes ($P = 3.1 \times 10^{-7}$); keratinocytes ($P = 3.1 \times 10^{-4}$); LCs and DCs ($P = 1.4 \times 10^{-4}$); and fibroblasts ($P = 4.0 \times 10^{-4}$). ***$P < 0.001$.

resolution provided by our large dataset to discern rare cell states (fig. S2, E and F). However, our analysis of interfollicular mammoplasty skin sampled to the top layer of the reticular dermis may not have adequately profiled all skin hair follicle and appendageal cells.

We selected genes encoding surface proteins (*CD8A*, *CD163*, *CD14*, and *CCR7*) and additional antigens (where antibodies were commercially available) to derive a cytometry by time-of-flight (CyTOF) panel for protein level validation and frequency assessment of the major cell states on four additional donors (fig. S3, A to E). Gene expression on the relevant cell states was consistent with CyTOF analysis (fig. S3F).

To evaluate the establishment of specific cell states during development and their temporal evolution in adult skin, we compared our adult skin scRNA-seq data with our embryonic/fetal [7 to 10 post-conception weeks (PCW); n = 7] scRNA-seq data (Fig. 1D) (*21*). We used the TransferAnchors function in Seurat to integrate adult and fetal skin cell states (Fig. 1E) (*22*) and calculated the proportional representation of the equivalent cell states in healthy developing and adult skin (Fig. 1F). Our collective dataset of human fetal, adult, and diseased skin cells provides a foundational resource and can be explored using an interactive web portal, https://developmentcellatlas.ncl.ac.uk/datasets/hca_skin_portal.

Transition from innate to adaptive lymphocytes during skin development

Skin T cells consist of three subtypes: cytotoxic (Tc) cells expressing *CD8A/B*, helper (T_H) cells expressing *CD4* and *CD40LG*, and regulatory (T_{reg}) cells expressing *FOXP3*, *TIGIT*, and *CTLA4* (Fig. 2, A and B) (*23*, *24*). We identified four clusters of innate lymphocytes in adult healthy skin that were CD161(*KLRB1*)$^+$CD3(*CD3D/CD3G*)$^-$, consisting of ILC1/3, ILC2, ILC1/natural killer (NK), and NK (*KLRD1*$^+$, *GNLY*$^+$, *PRF1*$^+$, *GZMB*$^+$, and *FCGR3A*$^+$) cells (Fig. 2, A and B). ILC1/NK cells have overlapping features of ILC1 and NK cells, as described (*25*, *26*). Plasticity within ILC1 and ILC3 is also recognized, as reflected in our annotation of ILC1/3 (*27*). ILC2 (*IL7R*, *PTGDR2*, and *GATA3*) has the most distinct signature in our data and in existing literature (Fig. 2B) (*26*).

In contrast to adult skin, the fetal skin lymphoid compartment is predominantly populated by ILCs (Fig. 1, D and F) between 7 and 10 PCW, prior to the development of the thymus, bone marrow, and spleen, where T and B lymphocytes differentiate. Fetal NK cells correlate with adult NK cells but express higher levels of *GZMM* and *GZMK* (Figs. 1E and 2B), which suggests that they may be functionally competent (*21*). Fetal skin ILCs (*IL7R*$^+$, *RORC*$^+$, and *KIT*$^+$) resemble adult skin ILC3 (Fig. 2B) (*28*).

To evaluate the impact of epidermal versus dermal microenvironment on T cells, we compared the differentially expressed genes of T cells in the two compartments (Fig. 2C). Epidermal T cells up-regulated the expression of genes associated with skin tissue residency (*RGS1* and *PPP1R15A*) (*29*), effector memory (*CD44* and *ID2*) (*29*, *30*), T cell activation (*TNFRSF18*) (*31*), and inhibition of T cell response (*CD96*, *TSC22D3*, and *DUSP4*) (*32*–*34*), in keeping with previous suggestions that resident memory T cells are poised to mount an effective immune response but express inhibitory molecules to prevent disadvantageous responses to nonpathogenic antigens (*35*). In contrast, dermal T cells express interferon-stimulated genes (*IFITM1*, *IFI6*, and *LY6E*) (*36*) and transcriptionally correlate closer to blood T cells than epidermal T cells do (fig. S4, A and B). Dermal T_{regs} show high mRNA and protein expression of the circulating central memory T cell marker CD62L (*SELL*) (Fig. 2C and fig. S3A).

Disease-associated and clonal T cells

In atopic dermatitis (AD), cytotoxic T cells expressing *IL13*, *IL22*, and *IFNG* (Tc IL13/IL22) are found in both lesional and nonlesional skin but are significantly enriched in lesional skin (P = 0.04, likelihood ratio test). Similarly, in psoriasis, T cells expressing *IL17A*, *IL17F*, *IFNG*, *IL22*, and *IL26* (Tc17/T_H17) are found in both lesional and nonlesional skin but are significantly enriched in lesional skin ($P < 0.001$, likelihood ratio test) (Fig. 2D and fig. S4C). Tc17/T_H17 cells are dominant in the epidermis of lesional psoriasis skin, as validated by flow cytometry (Fig. 2D and fig. S4D). These cells express genes characteristic of activated and pathogenic T_H17 cells (*KLRB1*, *RBPJ*, and *CXCL13*) (*37*–*39*) (fig. S4E). Tc IL13/IL22 cells are dominant in the dermis of AD lesional skin (Fig. 2D) and express amphiregulin (*AREG*, a member of the epidermal growth factor family) (*40*), skin tissue residency genes (*RGS1*, *NR4A1*, *NR4A2*) (*29*), and effector and activated T cell genes (*ID2*, *PRDM1*, *MAP3K8*, *DUSP2*) (*30*, *41*–*44*) (fig. S4E). To further extend our observation to a larger patient cohort, we used the AutoGeneS tool (*18*) to deconvolute cellular heterogeneity in published AD and psoriasis bulk RNA-seq data (*45*). In accordance with our findings, we observed the presence of a Tc IL13/IL22 signature in lesional AD skin and a Tc17/T_H17 signature in lesional psoriasis skin (Fig. 2E).

For both AD and psoriasis, there was a significantly higher proportion of T cell clones shared between nonlesional and lesional skin within donors versus between donors ($P <$ 0.01, two-sample t test) (fig. S4F). In AD and psoriasis lesional skin, disease-associated Tc IL13/22 and Tc17/T_H17 cells exhibited significantly higher clonality [$P < 0.05$ using quasi-binomial statistics to model proportions, followed by analysis of variance (ANOVA)] and the lowest diversity compared to T_H, T_{reg}, and Tc cell subsets (Fig. 2F and fig. S4G). Lesional clonal T cells had higher expression of co-stimulation genes (*CD63*, *TNFRSF18*, and *JAML*) and T cell receptor signaling (*EVL*, *LAT*, *LCK*, and *JAK1*) than did nonclonal T cells (Fig. 2G).

Mononuclear phagocytes in adult and developing skin

We observed 14 states of mononuclear phagocytes (MPs) in human skin (Fig. 3, A and B, and fig. S5A) that we annotated by aligning skin and blood MPs using the TransferAnchors function in Seurat (fig. S5B) and expression of MP marker genes (*46*) (fig. S5C). This work revealed the limitations of currently used surface markers and FACS gates to adequately resolve skin MP heterogeneity (fig. S5A).

Two macrophage cell states expressing *CD68* are present in healthy skin. Mac1 shows higher expression of complement transcripts (*C1QB* and *C1QC*) and scavenger receptors (*CD163* and *MARCO*), whereas Mac2 is characterized by the expression of *F13A1* and transcription factors associated with alternative activation and suppression of immune responses (*NR4A1*, *NR4A2*, and *KLF4*) (Fig. 3B and fig. S5C) and, notably, is more closely aligned with fetal macrophages (Fig. 1E).

We observed dendritic cells 1 and 2 (DC1, DC2) and Langerhans cells (LCs) in embryonic skin as early as 7 PCW, prior to bone marrow hematopoiesis, but macrophages were the dominant MP in first-trimester skin (Fig. 1, D to F, and fig. S5D). Interestingly, embryonic/fetal LCs are enriched for macrophage-related genes such as *C1QC*, *FCGR2A*, and *CTSB* (Fig. 3B) and correlate poorly with adult LCs (Fig. 1E). This lends support to a differential origin of prenatal LCs from yolk sac and fetal liver progenitors, as previously reported in mice (*47*), in contrast to the bone marrow–derived hematopoietic stem cell origin of some adult human LCs (*48*).

Migratory dendritic cell signature is conserved across species and augmented in disease states

In the steady state, skin dendritic cells (DCs) undergo a continual process of homeostatic maturation that is required for the induction of tolerance to innocuous environmental antigens (*49*). This is accompanied by their migration to skin draining lymph nodes through lymphatic vessels, a process dependent on CCR7 (*13*). Partition-based approximate graph abstraction (PAGA) analysis revealed three branches of differentiation: LCs, myeloid DCs (DC1 and DC2), and monocyte-derived DCs (moDCs) (Fig. 3C). The clusters at the convergence of these branches [moDC3, LC4, and migratory

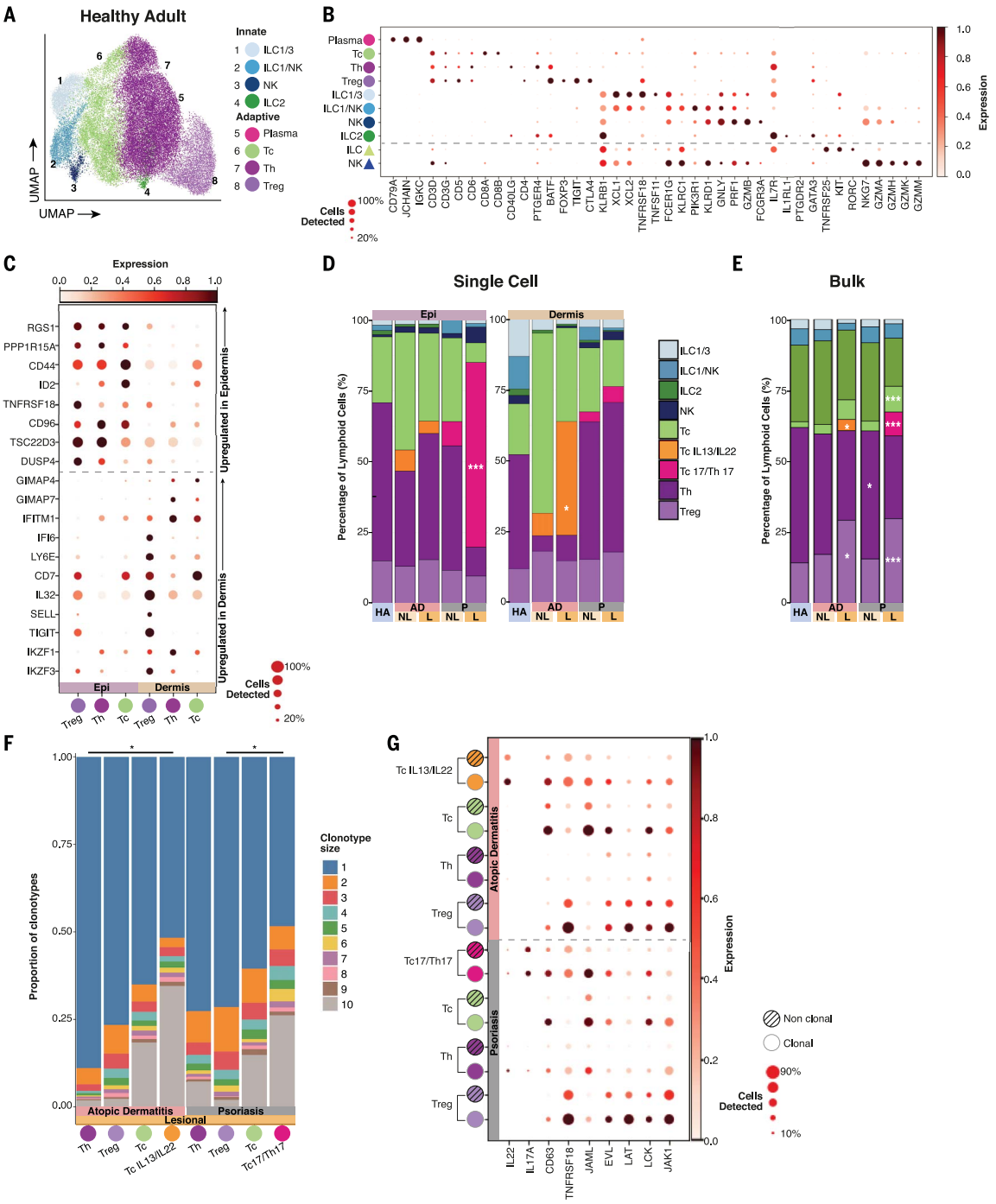

Fig. 2. Skin innate lymphoid cells, T lymphocytes, and T cell receptor analysis. (**A**) UMAP visualization of lymphoid cells in healthy adult skin (n = 5). ILC, innate lymphoid cell; NK, natural killer cell; Tc, cytotoxic T cell; T_H, T helper cell, T_{reg}, regulatory T cell. (**B**) Dot plot showing expression of marker genes of cell states found in adult skin (circles) shown in (A) and their developmental counterparts (triangles), separated by the dashed line. (**C**) Dot plot showing the differentially expressed genes in T cell subsets between epidermis and dermis in healthy adult skin (n = 5). Epi, epidermis. (**D**) Bar charts showing the proportions of lymphoid cell states in healthy and diseased skin. Tc IL13/IL22, cytotoxic T cells expressing *IL13* and *IL22*; Tc17/T_H17, T cells expressing *IL17A* and *IL17F*. Lesional dermal AD skin Tc IL13/IL22 was compared to nonlesional dermal AD skin (modeled counts as negative binomial and analyzed by ANOVA, *P = 0.04); psoriasis epidermal lesional skin Tc17/T_H17 was compared to psoriasis nonlesional epidermis (***P < 0.001). Significance of other cell states was not tested. HA, healthy adult; AD, atopic dermatitis; P, psoriasis; L, lesional; NL, nonlesional. (**E**) Proportion of cells with Tc IL13/IL22 and Tc17/T_H17 signatures present in bulk RNA-seq data from GSE121212. Modeling the data on a quasibinomial distribution, lesional AD is enriched for Tc IL13/IL22 ($P = 3.4 \times 10^{-2}$) and T_{reg} ($P = 3.2 \times 10^{-2}$) relative to nonlesional skin. Lesional psoriasis is enriched for Tc17/T_H17 ($P = 1.6 \times 10^{-5}$), T_{reg} ($P = 4.6 \times 10^{-7}$), and Tc ($P = 2.5 \times 10^{-4}$) relative to nonlesional. P values were calculated using a likelihood ratio test. (**F**) Bar charts showing clonotype size in each T cell subset in lesional AD (left) and psoriasis (right). The color of the bar relates to the size of the clonotype. Modeling the data on a quasibinomial distribution, lesional AD dermis Tc IL13/IL22 cells have a higher proportion of clonotypes with ≥2 cells relative to T_H ($P = 3.3 \times 10^{-2}$), and lesional psoriasis Tc17/T_H17 cells have a higher proportion of clonotypes with ≥2 cells than do T_{regs} ($P = 1.6 \times 10^{-2}$); other comparisons were not significant. P values were calculated using a likelihood ratio test. Bars across the top show significance between cell types. (**G**) Dot plot showing the expression of genes that were significantly differentially expressed between nonclonal and clonal T cells in AD (top) and psoriasis (bottom). Hatched and solid colored circles indicate nonclonal and clonal T cells, respectively. *P < 0.05, ***P < 0.001.

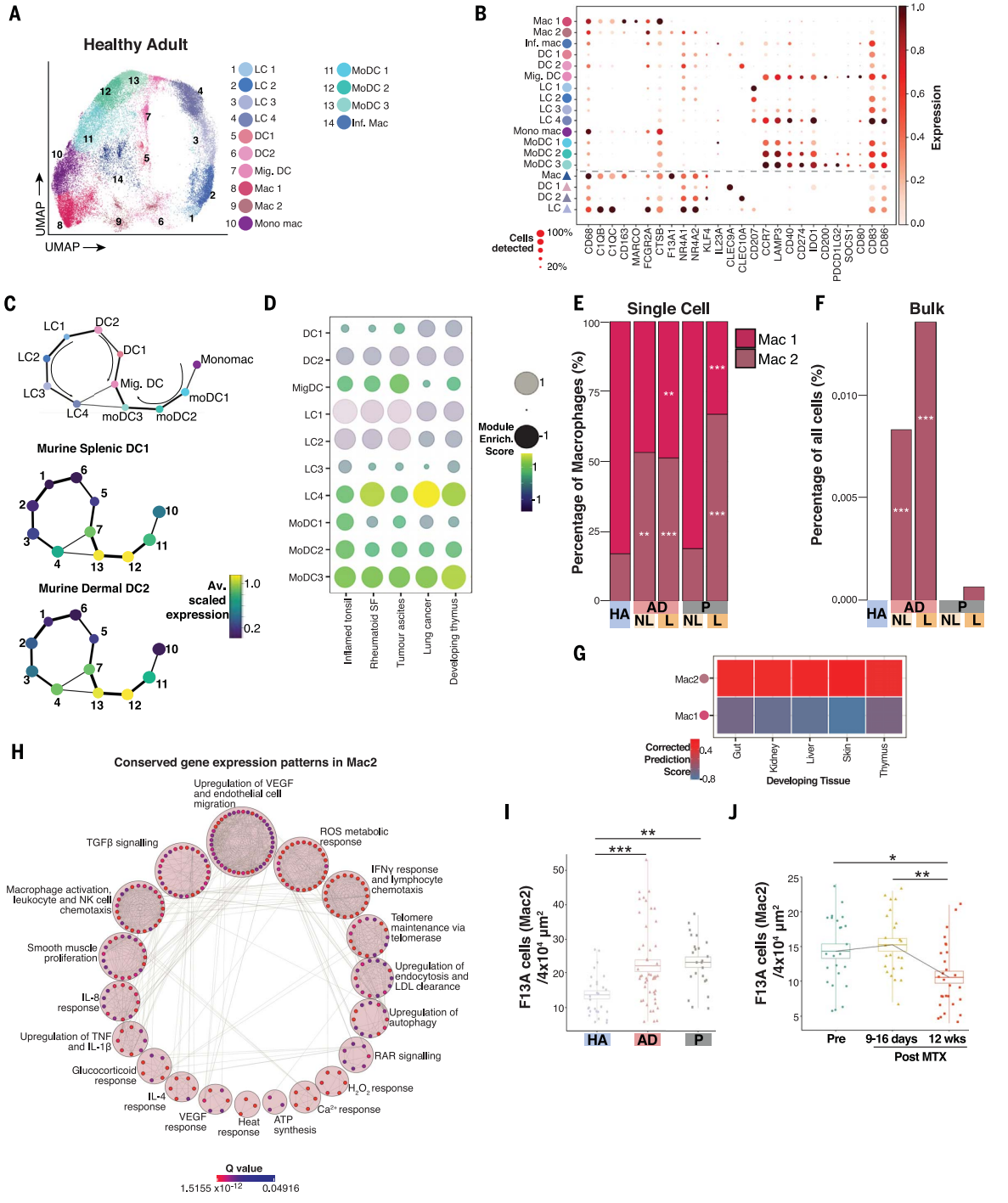

Fig. 3. Dermal and epidermal mononuclear phagocytes. (**A**) UMAP visualization of different antigen-presenting cell (APC) states found in healthy adult skin (n = 5). See Fig. 1B for abbreviations. (**B**) Dot plot showing the expression of differentially expressed genes characterizing adult healthy skin cell states (circles) shown in (A) and their developmental counterparts (triangles), separated by the dashed line. (**C**) Top: Abstracted graph (PAGA) showing connectivity between adult healthy skin DC clusters. The size of the nodes is proportional to cluster size; edge thickness is proportional to the strength of the connection between nodes. Bottom: enrichment of gene signatures for murine splenic Xcr1$^+$DC (DC1) and dermal CD11c$^+$ (DC2) in each node. Av, average. (**D**) Dot plot of enrichment of gene signature of APC cell types in adult human disease and in the developing thymus. SF, synovial fluid. (**E**) Bar charts showing the proportions of Mac1 and Mac2 in adult healthy, AD, and psoriasis skin. HA, healthy adult; AD, atopic dermatitis; P, psoriasis; L, lesional; NL, nonlesional. Mac2 cells are significantly expanded in both lesional AD and psoriasis skin, and Mac1 cells are significantly reduced in both lesional AD and psoriasis skin [Mac1, $P = 5.4 \times 10^{-3}$ (AD lesional), 3.3×10^{-5} (psoriasis lesional); Mac2, $P = 6.3 \times 10^{-3}$ (AD nonlesional), 6.0×10^{-5} (AD lesional), 1.4×10^{-6} (psoriasis lesional)]. P values were calculated using a likelihood ratio test. (**F**) Proportion of cells with Mac2 signature present in bulk RNA-seq data from GSE121212. We used generalized linear modeling on a quasibinomial distribution to compare proportions of predicted Mac2 cells between healthy and lesional skin and showed statistically significant expansion of Mac2 in lesional AD ($P = 1.7 \times 10^{-7}$). P values were calculated using a likelihood ratio test. (**G**) Prediction score for alignment using CCA (Seurat) between developing gut, kidney, liver, skin, and thymus macrophages with Mac1 and Mac2 in healthy adult skin. (**H**) Network visualizations of pathways conserved between developing skin macrophages and Mac2 in AD and psoriasis. Network nodes are colored by enrichment score ($q < 0.05$) and represent individual enriched gene sets; edges represent genes shared between nodes (intersect ≥10%). (**I**) Jitter plot displaying the number of positive F13A cells in 4×10^4 µm^2 of healthy adult (n = 7), AD (n = 12), and psoriasis (n = 6) skin (P between healthy adult and AD = 6.6×10^{-4} ; P between healthy adult and psoriasis = 1.2×10^{-3}). (**J**) Jitter plot displaying the number of positive F13A cells in 4×10^4 µm^2 of AD skin (n = 5) before treatment with methotrexate and 9 to 16 days and 12 weeks post-treatment (P between pretreatment and 12 days post-treatment = 1.5×10^{-2}; P between 9 to 16 days and 12 weeks post-treatment = 2.0×10^{-3}). *$P < 0.05$, **$P < 0.01$, ***$P < 0.001$.

DC (Mig. DC)] express transcripts associated with DC maturation (*CD83*, *CCR7*, *LAMP3*, *CD40*, and *CD86*), immunoregulation (*CD274*, *IDO1*, *CD200*, *PDCD1LG2*, and *SOCS1*) (Fig. 3B and table S1) (*50*), and migration (*FSCN1*, *PLGRKT*, *TRAF1*, *BCL2A1*, *CFLAR*, and *REL*) (Fig. 3C) as in migratory murine dermal DC2 and splenic DC1 (*49*, *51*, *52*). Acquisition of this common gene signature is associated with loss of genes conferring subset identity in mice (*53*), which we also observe here for moDC3, LC4, and Mig. DC (Fig. 3B).

Surprisingly, the migratory DC signature is also present across disease states including tonsillitis, ascites (*53*, *54*), lung cancer (*50*), and rheumatoid arthritis (Fig. 3D). We previously reported the expression of migratory genes in fetal thymic medullary DCs (*55*), which suggests that developmental gene programs are used in adult tissue homeostasis and augmented in disease.

Fetal macrophage program in AD and psoriasis

We observed an increase in Mac2 in AD and psoriasis skin (Fig. 3E and fig. S5E), which was corroborated in a larger patient bulk RNA-seq dataset (Fig. 3F). Adult healthy skin Mac2 aligned with fetal skin, gut, kidney, liver, and thymus macrophages (Fig. 3G). This led us to hypothesize a cellular program shared between fetal macrophages in AD skin and Mac2 cells in psoriasis skin, which are significantly differentially expressed relative to other skin cells. We derived 91 significantly conserved genes (Seurat FindConservedMarkers using negative binomial test, $P < 0.05$) between analogous macrophage clusters in developing skin and lesional AD and psoriasis skin (table S5). This revealed genes related to stress (*DNAJB1*, *HSPA1B*, *HSPA1A*, *JUN*, and *FOSB*), chemotactic (*CCL4L2*, *CCL4*, *CCL3L1*, and *CCL3*), and angiopoietin (*EGR1* and *PTGS2*) signaling. Gene Ontology analysis revealed significantly enriched gene set clusters (hypergeometric test q value < 0.05) relating to the regulation of angiogenesis, leukocyte chemotaxis, and transforming growth factor–β (TGF-β) signaling (Fig. 3H and table S6). The role of macrophages in tissue homeostasis and regeneration is gaining recognition (*56*). Our findings add insight into how macrophage programs that support angiogenesis and leukocyte seeding in tissues during fetal development reemerge during AD and psoriasis pathogenesis.

To confirm the role of Mac2 in disease pathogenesis in vivo, we analyzed the abundance of Mac2 in healthy, AD, and psoriasis lesional skin, as well as during AD resolution resulting from systemic treatment with methotrexate (Fig. 3, I and J). We leveraged the marker F13A for Mac2 from our scRNA-seq data (Fig. 3B) and enumerated F13A-expressing Mac2 cells by immunohistochemistry. This revealed a significant increase in Mac2 in AD and psoriasis lesional skin relative to healthy skin, as well as a decline in Mac2 12 weeks after commencement of methotrexate treatment, in parallel with a reduction in patients' clinical Eczema Area and Severity Index (EASI) score (Fig. 3J and fig. S5F).

In both AD and psoriasis, LC1 has the highest enrichment of cell cycle genes (fig. S5, G and H). To validate our findings, we examined LC proliferation in healthy, AD, and psoriasis epidermis. We found that $Ki67^+$ $Langerin^+$ cells increased in AD and psoriasis lesional skin (fig. S5I), consistent with previous findings (*57*, *58*). Using FACS index data, we determined that LC1 is enriched within the $Langerin^+CD1a^{lo}CD11c^{lo}$ gate distinct from $Langerin^+CD1a^{hi}$ LCs (fig. S5A). In contrast, epidermal $HLA\text{-}DR^+CD1a^-ang^-CD11c^+CD1c^+$ cells are predominantly moDCs and correspond with non–LC-like epidermal cells potent at stimulating T cell proliferation, proinflammatory cytokine production, and transmission of HIV to $CD4^+$ T cells (*59*).

Keratinocyte differentiation in healthy and diseased skin

We characterized four groups of keratinocytes: undifferentiated, proliferating, differentiated, and inflammatory differentiated cells (differentiated KC*) (Fig. 4A). Undifferentiated keratinocytes transcribe basal epidermal proteins (*KRT5* and *KRT14*) and are abundant in the $CD49f^{hi}$ FACS gate (Fig. 1C). Proliferating keratinocytes ($CDK1^+$ and $PCNA^+$) have lower expression of suprabasal cell transcripts (e.g., *KRT1*, *KRT10*) that characterize differentiated keratinocytes (Fig. 4B). Inflammatory differentiated keratinocytes coexpress lower levels of undifferentiated (*TP63* and *ITGA6*) and differentiated (*KRT1* and *KRT10*) transcripts but additionally express *ICAM1*, *TNF*, and *CCL20* (Fig. 4B). The gene expression patterns of these keratinocyte subgroups are in agreement with their spatial arrangement in the epidermis (Fig. 4C) (Human Protein Atlas, www.proteinatlas.org) and with a human epidermal scRNA-seq dataset (*60*) (fig. S6A). First-trimester human epidermis, comprising "basal" undifferentiated keratinocyte progenitors overlaid by the periderm, expresses keratin genes and proteins of simple epithelium (keratins 8, 18, and 19) (Fig. 4B and fig. S6B) (*61*).

Force-directed graph (FDG) and PAGA analyses revealed dual inferred differentiation trajectories from the stem cell gene (*TP63*, *PPP3CA*, and *CAV1/2*)–enriched basal keratinocytes into terminally differentiated keratinocytes expressing *CNFN*, *FLG*, and *IVL* (Fig. 4D, fig. S6C, and table S1) (*61*, *62*). One arm expresses high levels of lamellar body (LB)–related transcripts such as *ABCA12*, *CKAP4*, and *CLIP1* that characterize late epidermal differentiation, and the other arm expresses lower levels of LB-related transcripts (*63*) (Fig. 4E). *IRF1* and *SOX9*, transcription factors that are differentially expressed in the two pathways (fig. S6D), mark distinct cells by immunofluorescence analysis of healthy skin (Fig. 4F and fig. S6E). The statistically significant differentially expressed genes identified with Monocle (*64*) across keratinocyte differentiation (fig. S6C) recapitulate previous reports in human and mouse (*65*).

Notably, keratinocytes expressing LB-related transcripts coexpress genes associated with autosomal recessive congenital ichthyosis, such as *ABCA12*, *NIPAL4*, *SLC27A4*, and *TGM1* (Fig. 4E). However, analysis of fetal keratinocytes showed little to no expression of these congenital ichthyosis-related genes, which suggests that disease onset at the molecular level begins only after 10 PCW (Fig. 4E). This is in keeping with the absence of a granular layer in first-trimester fetal epidermis, where *LOR*, *FLG*, *IVL*, and genes required for lamellar body production are expressed (*65*, *66*). Inflammatory differentiated keratinocytes express higher levels of genes associated with inflammatory ichthyoses and severe atopy, such as *NIPAL4* and *SPINK5* (Fig. 4E, cluster 8) (*67*).

Both AD and psoriasis lesional skin were enriched for differentiated keratinocytes (Fig. 4G), as supported by deconvolution of bulk RNA-seq data from an extended patient cohort (Fig. 4H). Differentially expressed gene analysis revealed lower expression of stem cell and basal keratinocyte genes (*CAV1/2*, *KRT14*, and *DUSP10*) but higher expression of commitment genes (*FOS*, *JUNB*, *CDKN1A*, *MAFB*) in undifferentiated lesional psoriasis and AD keratinocytes (fig. S6F). These observations agree with previous reports (*68*, *69*) and suggest rapid transition and differentiation of keratinocytes in AD and psoriasis lesional skin. Lesional differentiated keratinocytes additionally expressed inflammatory transcripts including alarmins (*S100A7*, *S100A8*, *S100A9*), serpins (*SERPINB4*, *SERPINB13*), and interferon response genes (*IFI27*, *IFITM1*) (fig. S6F). The proportion of inflammatory differentiated keratinocytes, resembling previously described CCL20-expressing keratinocytes in murine inflammatory skin disease induced by subcutaneous interleukin-17 (IL-17) and tumor necrosis factor (TNF-α) injection (*70*), are expanded in psoriasis skin (Fig. 4G).

Stromal cell heterogeneity

We next interrogated the heterogeneity within fibroblasts, vascular and lymphatic endothelial cells, and Schwann cells (Fig. 5, A and B). Fibroblasts dominated the nonimmune cell population in developing skin; the proportional representation of melanocytes, Schwann cells, and lymphatic and vascular endothelial cells was increased in adult skin (Fig. 1F).

Three fibroblast subsets expressing extracellular matrix (ECM)–related genes such as

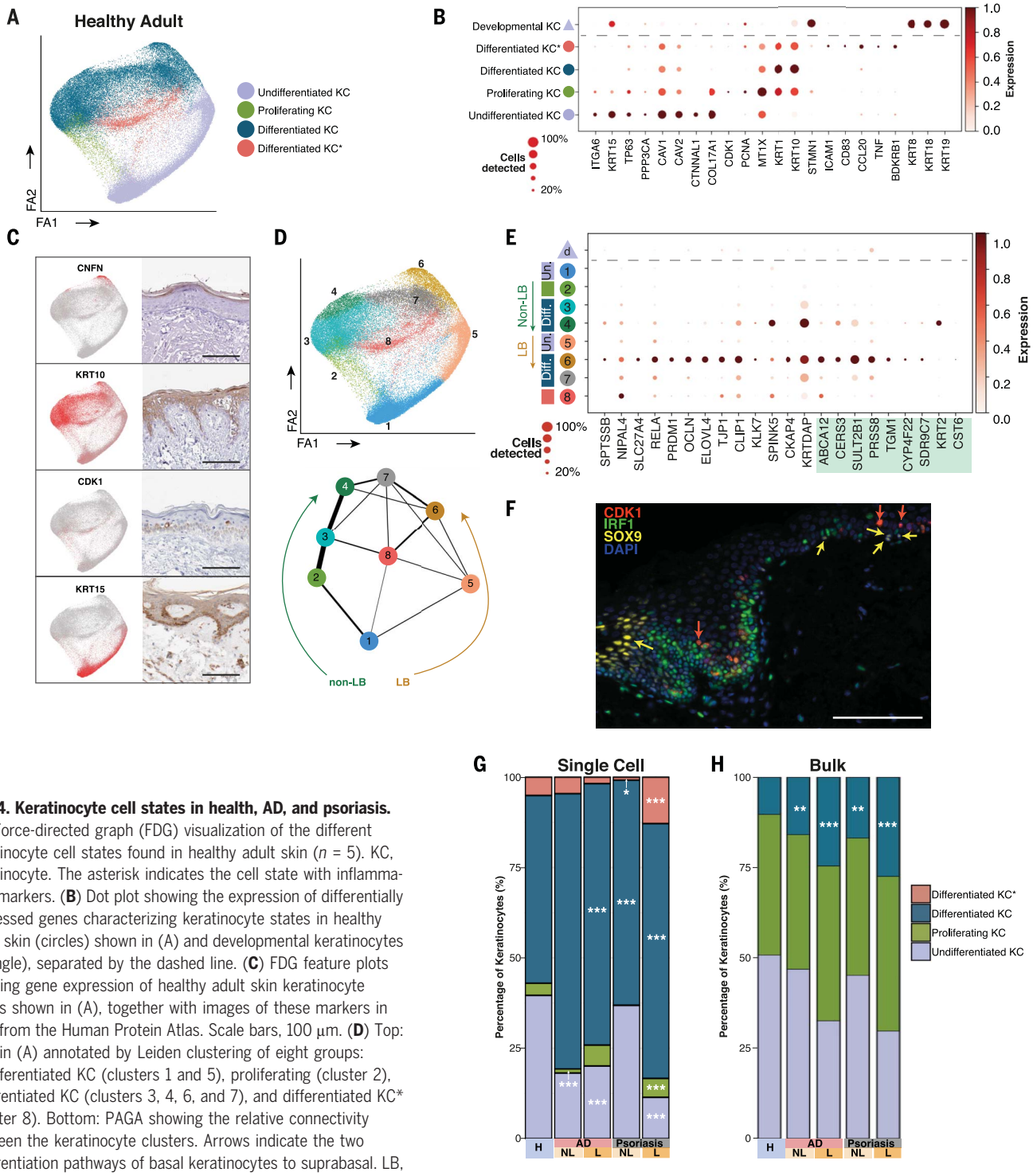

Fig. 4. Keratinocyte cell states in health, AD, and psoriasis. (**A**) Force-directed graph (FDG) visualization of the different keratinocyte cell states found in healthy adult skin (n = 5). KC, keratinocyte. The asterisk indicates the cell state with inflammatory markers. (**B**) Dot plot showing the expression of differentially expressed genes characterizing keratinocyte states in healthy adult skin (circles) shown in (A) and developmental keratinocytes (triangle), separated by the dashed line. (**C**) FDG feature plots showing gene expression of healthy adult skin keratinocyte states shown in (A), together with images of these markers in situ, from the Human Protein Atlas. Scale bars, 100 μm. (**D**) Top: FDG in (A) annotated by Leiden clustering of eight groups: undifferentiated KC (clusters 1 and 5), proliferating (cluster 2), differentiated KC (clusters 3, 4, 6, and 7), and differentiated KC* (cluster 8). Bottom: PAGA showing the relative connectivity between the keratinocyte clusters. Arrows indicate the two differentiation pathways of basal keratinocytes to suprabasal. LB, lamellar body. (**E**) Dot plot of genes related to lamellar body production and ichthyosis (green box) expressed by healthy adult keratinocyte states (circles) shown in (D), as well as fetal keratinocytes (triangle). Un., undifferentiated; Diff., differentiated. (**F**) Immunofluorescence staining of healthy adult skin for CDK1 (red), IRF1 (green), SOX9 (yellow), and DAPI (blue). Red and yellow arrows indicate CDK1$^+$ and SOX9$^+$ cells, respectively, in suprabasal layers. Image is representative of n = 3 donors. Scale bar, 100 μm. (**G**) Bar charts showing the proportions of the keratinocyte cell states in healthy and diseased skin. Undifferentiated KCs, $P = 6.1 \times 10^{-4}$ (AD lesional), 3.0×10^{-5} (psoriasis lesional); differentiated KCs, $P = 6.5 \times 10^{-16}$ (AD lesional), 6.5×10^{-7} (psoriasis nonlesional), 8.8×10^{-20} (psoriasis lesional); differentiated KCs*, $P = 2.3 \times 10^{-2}$ (psoriasis nonlesional), 1.5×10^{-4} (psoriasis lesional); proliferating KCs, $P = 6.5 \times 10^{-10}$ (AD nonlesional), 8.1×10^{-14} (psoriasis lesional). Populations are compared to those in healthy adults. P values were calculated using a likelihood ratio test. (**H**) Percentage of cells with undifferentiated, differentiated, and proliferating keratinocyte signatures present in bulk RNA-seq data from GSE121212. Generalized linear modeling on a quasibinomial distribution was used to compare proportions of predicted keratinocyte subsets between healthy, nonlesional, and lesional skin and showed statistically significant expansion of differentiated keratinocytes in nonlesional AD ($P = 1.1 \times 10^{-3}$), lesional AD ($P = 9.6 \times 10^{-10}$), nonlesional psoriasis ($P = 2.1 \times 10^{-5}$), and lesional psoriasis ($P = 2.0 \times 10^{-16}$). *$P < 0.05$, **$P < 0.01$, ***$P < 0.001$.

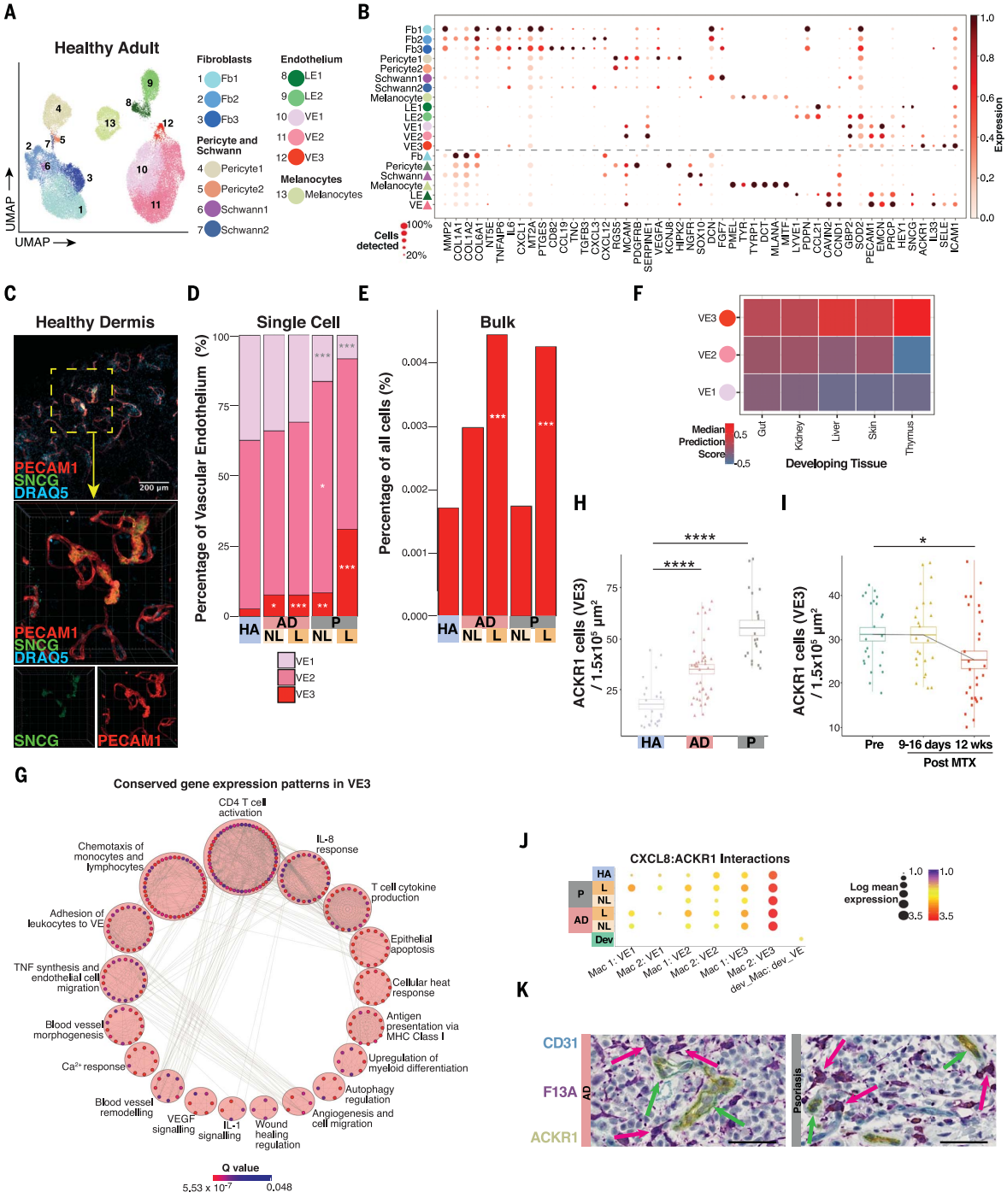

Fig. 5. Stromal and endothelial cells. (**A**) UMAP visualization of the nonimmune, non-keratinocyte cell states found in healthy adult skin (n = 5). Fb, fibroblast; LE, lymphatic endothelium; VE, vascular endothelium. (**B**) Dot plot showing the expression of differentially expressed genes characterizing adult healthy skin cell states (circles) shown in (A) and their developmental counterparts (triangles), separated by the dashed line. (**C**) 3D reconstruction of Z-stacked images of whole-mount immunofluorescence staining of dermis for CD31 (PECAM1, red), γ-synuclein (SNCG, green), and DRAQ5 (blue). White cube outlined in central image represents 40 µm × 40 µm × 40 µm. (**D**) Bar charts showing the proportions of VE in healthy adult and diseased skin [VE1, $P = 5.5 \times 10^{-6}$ (psoriasis nonlesional), 5.0×10^{-15} (psoriasis lesional); VE2, $P = 1.9 \times 10^{-2}$ (psoriasis nonlesional); VE3, $P = 1.3 \times 10^{-2}$ (AD nonlesional), 1.5×10^{-4} (AD lesional), 1.3×10^{-3} (psoriasis nonlesional), 6.2×10^{-9} (psoriasis lesional)]. P values were calculated using a likelihood ratio test. (**E**) Proportion of cells with VE3 signature present in bulk RNA-seq data from GSE121212. The proportion of VE3 increased in both lesional AD ($P = 9.1 \times 10^{-4}$) and psoriasis ($P = 8.2 \times 10^{-4}$). P values were calculated using a likelihood ratio test. (**F**) Prediction score for alignment using CCA (Seurat) between developing gut, kidney, liver, skin, and thymus VE with VE1, VE2, and VE3 in healthy adult skin. (**G**) Network visualization of pathways conserved between developing skin VE and VE3 in AD and psoriasis. Network nodes are colored by enrichment score ($q < 0.05$) and represent individual enriched gene sets; edges represent genes shared between nodes (intersect ≥10%). (**H**) Jitter plot displaying the number of positive ACKR1 cells in 1.5×10^5 µm^2 of healthy adult (n = 6), AD (n = 12), and psoriasis (n = 6) skin (ANOVA P value between healthy adult and AD, 3.0×10^{-5}; between healthy adult and psoriasis, 2.4×10^{-13}). (**I**) Jitter plot displaying the number of positive ACKR1 cells in 1.5×10^5 µm^2 of AD skin (n = 5) before treatment with methotrexate and 9 to 16 days and 12 weeks post-treatment (ANOVA P value between pretreatment and 12 weeks post-treatment, 5.0×10^{-2}). (**J**) Interactions between macrophage and vascular endothelium subsets predicted by CellPhoneDB. Color and size indicate $\log_2$ mean expression, averaged across the two clusters. Dev, developing skin. (**K**) Immunohistochemical staining of AD (left) and psoriasis (right) skin for F13A (purple), ACKR1 (yellow), and CD31 (teal), showing the close proximity of Mac2 and VE3. Pink arrows point to F13A-positive macrophages; green arrows point to CD31/ACKR1-positive vascular endothelial cells. Scale bars, 20 µm. Representative images from n = 4 for AD and n = 6 for psoriasis are shown. *$P < 0.05$, **$P < 0.01$, ***$P < 0.001$.

MMP2, *COL1A1*, *COL1A2*, and *NT5E* (encodes CD73) are present in healthy human skin, dominated by Fb1 fibroblasts with minor populations of Fb2 and Fb3 fibroblasts (Fig. 5, A and B). Dermal fibroblast heterogeneity encompassing structural and immunomodulatory subtypes has been previously reported at the single-cell level (*6*, *8*). Interestingly, fibroblasts in fetal skin express more genes relating to Fb2 adult fibroblasts, including *COL1A1*, *COL1A2*, and *COL6A1*, which suggests that they are functionally specialized toward ECM remodeling and maintenance (Fig. 5B). Furthermore, in AD and psoriasis lesional and nonlesional skin, Fb2 fibroblasts are significantly enriched relative to healthy skin and have up-regulated expression of the chemokines *CXCL12* and *CCL19*, in keeping with recent reports (*71*) (fig. S7, A and B).

Specialized vascular endothelium mediates leukocyte trafficking

Endothelial cells in the healthy adult dermis constitute the vascular endothelium (*PECAM1*, *EMCN*) and lymphatic endothelium (*LYVE1*, *PDPN*) (Fig. 5, A and B, and table S1). There are two subclusters of lymphatic endothelial cells defined by the differential expression of *CCL21* and *PDPN*, which are higher in LE1 and LE2, respectively (Fig. 5, A and B), the latter resembling $PDPN^+$ collecting lymphatic vessels in human dermis (*14*). Notably, LE1 cells express higher levels of the chemoattractant *CCL21*, which mediates DC migration into skin draining lymph nodes, as well as angiogenesis factors *CAVIN2* and *CCND1*, further supporting their function as initial afferent lymphatics (*72*) (Fig. 5B and table S1).

Three distinct states of *PECAM1* (CD31)–expressing vascular endothelial cells (VE1, VE2, VE3) are present in adult dermis. VE3, which forms ~2% of endothelial cells, is characterized by γ-synuclein (*SNCG*) and high expression of the venular capillary marker *ACKR1* (*73*, *74*) (Fig. 5B). In addition, VE3 cells coexpress inflammatory cytokines, chemokines, and leukocyte adhesion molecules including *IL6*, *IL33*, *SELE*, and *ICAM1* (Fig. 5B), similar to lymph node high endothelial venules that mediate leukocyte entry (*75*, *76*). We performed whole-mount immunostaining of healthy dermis and identified $SNCG^+PECAM1^+$(VE3) distended vascular structures in the superficial dermis (Fig. 5C), which suggests that these cells may be postcapillary venular cells regulating leukocyte adhesion and migration.

Co-optation of developmental gene programs in AD and psoriasis

We observed significant expansion of VE3 in AD and psoriasis lesional skin (Fig. 5D and fig. S7B) that was also evident in the broader patient cohort bulk RNA-seq data (Fig. 5E). Fetal skin VE cells aligned transcriptionally with adult skin VE3 and also expressed genes involved in leukocyte adhesion and trafficking (Figs. 1E and 5B). The expansion of VE3 in inflamed skin and transcriptome alignment of fetal gut, kidney, liver, skin, and thymus VE and of adult skin VE3 (Fig. 5F) led us to hypothesize that developmental VE gene programs are involved in AD and psoriasis pathogenesis, similar to our earlier observation with Mac2. We derived 112 genes that were conserved (Seurat FindConservedMarkers, negative binomial test, $P < 0.05$) between fetal skin VE and AD and psoriasis VE3. This identified gene sets related to stress (*DNAJB1*, *HSPA6*, *HSPB1*, *HSPH1*, *HSP90AA1*), IL-6 (*SOCS3*), and angiopoietin (*EGR1*) signaling, similar to Mac2 (tables S5 and S6). Gene Ontology analysis identified significantly enriched gene set clusters (hypergeometric test, q value < 0.05), similar to Mac2 (Figs. 3H and 5G), relating to leukocyte adhesion, T cell activation, and IL-8 response as conserved gene modules in developing skin VE and VE3 in AD and psoriasis, respectively (Fig. 5G and table S6).

To validate the pathogenic role of VE3 in inflammatory skin disease in vivo, we used ACKR1 as a marker for VE3 (based on the scRNA-seq data of healthy, AD, and psoriasis skin) (Fig. 5B and fig. S7C) and compared the abundance of VE3 in healthy, AD, and psoriasis skin before and after treatment with oral methotrexate. This showed a significantly higher ($P < 0.05$, ANOVA) frequency of VE3 in AD and psoriasis skin and a reduction in VE3 in the skin of AD patients after treatment, in line with clinical response and reduction in EASI score, similar to Mac2 (Fig. 5, H and I). Flow cytometry analysis also confirmed the expansion of VE3 in lesional psoriasis skin (fig. S7, D and E).

Mac2 and VE3 are the only skin cell states significantly enriched for these leukocyte migration gene programs; hence, we investigated whether they were interacting with each other or other immune cells to coordinate this function. To assess cell-cell interactions in healthy, AD, and psoriasis skin, we interrogated the CellPhoneDB receptor-ligand database, which predicted a significant enrichment for *ACKR1* on VE3 to interact with *CXCL8* (IL-8) on Mac2 (Fig. 5J and fig. S7F). We confirmed this cell-cell interaction in situ, demonstrating the close apposition of VE3 and perivascular Mac2 in AD and psoriasis skin (Fig. 5K). CellPhoneDB analysis also predicted enhanced interaction between both VE3 and Mac2 with lymphocytes in AD and psoriasis skin relative to healthy skin, supporting a role for these cells in lymphocyte recruitment into inflamed skin (fig. S7G).

Discussion

The importance of developmental programs in carcinogenesis and metastasis of both childhood and adult-onset tumors is well established (*1*, *2*, *77*). The impact of developmental programs in adult-onset neurodegenerative disorders is also emerging (*78*). Our findings support a broader use of prenatal cellular programs, not only in inflammatory skin disease but also potentially in other immune-mediated inflammatory disorders. Lymphocyte seeding into the developing skin is reliant on the structural network provided by the vasculature and, as our data suggest, also through endothelial cell interactions with macrophages (*21*), which are the most abundant skin-resident immune cells during embryonic development. We postulate that this interplay is co-opted to recruit immune cells in inflammatory skin disease. The molecular regulation of conserved gene modules during development may be distinct from that observed in disease. Dissecting the precise interplay of known angiogenic triggers, such as hypoxia, Wnt, STAT3, and β-catenin signaling, will pave the way toward a mechanistic understanding of VE3 expansion. Establishing the intrinsic and tissue-extrinsic factors that drive the Mac2 state acquisition in disease may innovate anti-inflammatory strategies. In addition to prenatal endothelial cell and macrophage gene programs, the skin fibroblast (F2) cell program is also augmented in AD and psoriasis, as well as activation of the fetal thymic medullary DC state in inflammation of several adult tissues and cancer (*50*, *53*–*55*).

Our human skin atlas provides a road map for targeting pathological programs in inflammatory skin diseases and is a foundational resource for the dynamic cutaneous cellular topology that evolves during fetal development, adulthood, and inflammation.

REFERENCES AND NOTES

1. S. Jessa *et al.*, Stalled developmental programs at the root of pediatric brain tumors. *Nat. Genet.* **51**, 1702–1713 (2019). doi: 10.1038/s41588-019-0531-7; pmid: 31768071
2. I. Tirosh *et al.*, Single-cell RNA-seq supports a developmental hierarchy in human oligodendroglioma. *Nature* **539**, 309–313 (2016). doi: 10.1038/nature20123; pmid: 27806376
3. R. Francis *et al.*, Gastrointestinal transcription factors drive lineage-specific developmental programs in organ specification and cancer. *Sci. Adv.* **5**, eaax8898 (2019). doi: 10.1126/sciadv.aax8898; pmid: 31844668
4. M. M. Pomerantz *et al.*, Prostate cancer reactivates developmental epigenomic programs during metastatic progression. *Nat. Genet.* **52**, 790–799 (2020). doi: 10.1038/s41588-020-0664-8; pmid: 32690948
5. E. Guttman-Yassky, J. G. Krueger, Atopic dermatitis and psoriasis: Two different immune diseases or one spectrum? *Curr. Opin. Immunol.* **48**, 68–73 (2017). doi: 10.1016/j.coi.2017.08.008; pmid: 28869867
6. C. Philippeos *et al.*, Spatial and Single-Cell Transcriptional Profiling Identifies Functionally Distinct Human Dermal Fibroblast Subpopulations. *J. Invest. Dermatol.* **138**, 811–825 (2018). doi: 10.1016/j.jid.2018.01.016; pmid: 29391249
7. L. Solé-Boldo *et al.*, Single-cell transcriptomes of the human skin reveal age-related loss of fibroblast priming. *Commun. Biol.* **3**, 188 (2020). doi: 10.1038/s42003-020-0922-4; pmid: 32327715
8. T. Tabib, C. Morse, T. Wang, W. Chen, R. Lafyatis, SFRP2/DPP4 and FMO1/LSP1 Define Major Fibroblast Populations in Human Skin. *J. Invest. Dermatol.* **138**, 802–810 (2018). doi: 10.1016/j.jid.2017.09.045; pmid: 29080679
9. V. Vorstandlechner *et al.*, Deciphering the functional heterogeneity of skin fibroblasts using single-cell RNA sequencing. *FASEB J.* **34**, 3677–3692 (2020). doi: 10.1096/fj.201902001RR; pmid: 31930613

10. D. Xue, T. Tabib, C. Morse, R. Lafyatis, Transcriptome landscape of myeloid cells in human skin reveals diversity, rare populations and putative DC progenitors. *J. Dermatol. Sci.* **97**, 41–49 (2020). doi: 10.1016/j.jdermsci.2019.11.012; pmid: 31836271
11. M. Haniffa *et al*., Differential rates of replacement of human dermal dendritic cells and macrophages during hematopoietic stem cell transplantation. *J. Exp. Med.* **206**, 371–385 (2009). doi: 10.1084/jem.20081633; pmid: 19171766
12. M. Haniffa *et al*., Human tissues contain CD141^{hi} cross-presenting dendritic cells with functional homology to mouse CD103^{+} nonlymphoid dendritic cells. *Immunity* **37**, 60–73 (2012). doi: 10.1016/j.immuni.2012.04.012; pmid: 22795876
13. N. McGovern *et al*., Human dermal CD14^{+} cells are a transient population of monocyte-derived macrophages. *Immunity* **41**, 465–477 (2014). doi: 10.1016/j.immuni.2014.08.006; pmid: 25200712
14. X.-N. Wang *et al*., A three-dimensional atlas of human dermal leukocytes, lymphatics, and blood vessels. *J. Invest. Dermatol.* **134**, 965–974 (2014). doi: 10.1038/jid.2013.481; pmid: 24352044
15. See supplementary materials.
16. K. Polański *et al*., BBKNN: Fast batch alignment of single cell transcriptomes. *Bioinformatics* **36**, 964–965 (2020). pmid: 31400197
17. F. A. Wolf, P. Angerer, F. J. Theis, SCANPY: Large-scale single-cell gene expression data analysis. *Genome Biol.* **19**, 15 (2018). doi: 10.1186/s13059-017-1382-0; pmid: 29409532
18. H. Aliee, F. Theis, AutoGeneS: Automatic gene selection using multi-objective optimization for RNA-seq deconvolution. bioRxiv [preprint]. 23 February 2020.pmid: 940650
19. S. C. van den Brink *et al*., Single-cell sequencing reveals dissociation-induced gene expression in tissue subpopulations. *Nat. Methods* **14**, 935–936 (2017). doi: 10.1038/nmeth.4437; pmid: 28960196
20. R. A. Botting *et al*., Phenotypic and functional consequences of different isolation protocols on skin mononuclear phagocytes. *J. Leukoc. Biol.* **101**, 1393–1403 (2017). doi: 10.1189/jlb.4A1116-496R; pmid: 28270408
21. D.-M. Popescu *et al*., Decoding human fetal liver haematopoiesis. *Nature* **574**, 365–371 (2019). doi: 10.1038/s41586-019-1652-y; pmid: 31597962
22. T. Stuart *et al*., Comprehensive Integration of Single-Cell Data. *Cell* **177**, 1888–1902.e21 (2019). doi: 10.1016/j.cell.2019.05.031; pmid: 31178118
23. R. A. Clark, Resident memory T cells in human health and disease. *Sci. Transl. Med.* **7**, 269rv1 (2015). doi: 10.1126/scitranslmed.3010641; pmid: 25568072
24. B. V. Kumar, T. J. Connors, D. L. Farber, Human T Cell Development, Localization, and Function throughout Life. *Immunity* **48**, 202–213 (2018). doi: 10.1016/j.immuni.2018.01.007; pmid: 29466753
25. H. Spits, J. H. Bernink, L. Lanier, NK cells and type 1 innate lymphoid cells: Partners in host defense. *Nat. Immunol.* **17**, 758–764 (2016). doi: 10.1038/ni.3482; pmid: 27328005
26. M. L. Robinette *et al*., Transcriptional programs define molecular characteristics of innate lymphoid cell classes and subsets. *Nat. Immunol.* **16**, 306–317 (2015). doi: 10.1038/ni.3094; pmid: 25621825
27. J. H. Bernink *et al*., Interleukin-12 and -23 Control Plasticity of CD127^{+} Group 1 and Group 3 Innate Lymphoid Cells in the Intestinal Lamina Propria. *Immunity* **43**, 146–160 (2015). doi: 10.1016/j.immuni.2015.06.019; pmid: 26187413
28. E. Montaldo, K. Juelke, C. Romagnani, Group 3 innate lymphoid cells (ILC3s): Origin, differentiation, and plasticity in humans and mice. *Eur. J. Immunol.* **45**, 2171–2182 (2015). doi: 10.1002/eji.201545598; pmid: 26031799
29. J. Li, M. Olshansky, F. R. Carbone, J. Z. Ma, Transcriptional Analysis of T Cells Resident in Human Skin. *PLOS ONE* **11**, e0148351 (2016). doi: 10.1371/journal.pone.0148351; pmid: 26824609
30. K. D. Omilusik *et al*., Sustained Id2 regulation of E proteins is required for terminal differentiation of effector CD8^{+} T cells. *J. Exp. Med.* **215**, 773–783 (2018). doi: 10.1084/jem.20171584; pmid: 29440362
31. E. M. Esparza, R. H. Arch, Glucocorticoid-induced TNF receptor, a costimulatory receptor on naive and activated T cells, uses TNF receptor-associated factor 2 in a novel fashion as an inhibitor of NF-κB activation. *J. Immunol.* **174**, 7875–7882 (2005). doi: 10.4049/jimmunol.174.12.7875; pmid: 15944293
32. K. Stanko *et al*., CD96 expression determines the inflammatory potential of IL-9-producing Th9 cells. *Proc. Natl. Acad. Sci. U.S.A.* **115**, E2940–E2949 (2018). doi: 10.1073/pnas.1708329115; pmid: 29531070
33. C.-Y. Huang *et al*., DUSP4 deficiency enhances CD25 expression and CD4^{+} T-cell proliferation without impeding T-cell development. *Eur. J. Immunol.* **42**, 476–488 (2012). doi: 10.1002/eji.201041295; pmid: 22101742
34. E. Ayroldi *et al*., Modulation of T-cell activation by the glucocorticoid-induced leucine zipper factor via inhibition of nuclear factor κB. *Blood* **98**, 743–753 (2001). doi: 10.1182/blood.V98.3.743; pmid: 11468175
35. B. V. Kumar *et al*., Human Tissue-Resident Memory T Cells Are Defined by Core Transcriptional and Functional Signatures in Lymphoid and Mucosal Sites. *Cell Rep.* **20**, 2921–2934 (2017). doi: 10.1016/j.celrep.2017.08.078; pmid: 28930685
36. J. W. Schoggins, C. M. Rice, Interferon-stimulated genes and their antiviral effector functions. *Curr. Opin. Virol.* **1**, 519–525 (2011). doi: 10.1016/j.coviro.2011.10.008; pmid: 22328912
37. R. Ramesh *et al*., Pro-inflammatory human Th17 cells selectively express P-glycoprotein and are refractory to glucocorticoids. *J. Exp. Med.* **211**, 89–104 (2014). doi: 10.1084/jem.20130301; pmid: 24395888
38. G. Meyer zu Horste *et al*., RBPJ Controls Development of Pathogenic Th17 Cells by Regulating IL-23 Receptor Expression. *Cell Rep.* **16**, 392–404 (2016). doi: 10.1016/j.celrep.2016.05.088; pmid: 27346359
39. R. Takagi *et al*., B cell chemoattractant CXCL13 is preferentially expressed by human Th17 cell clones. *J. Immunol.* **181**, 186–189 (2008). doi: 10.4049/jimmunol.181.1.186; pmid: 18566383
40. T. B. Rojahn *et al*., Single-cell transcriptomics combined with interstitial fluid proteomics defines cell type-specific immune regulation in atopic dermatitis. *J. Allergy Clin. Immunol.* **146**, 1056–1069 (2020). doi: 10.1016/j.jaci.2020.03.041; pmid: 32344053
41. S. L. Nutt, K. A. Fairfax, A. Kallies, BLIMP1 guides the fate of effector B and T cells. *Nat. Rev. Immunol.* **7**, 923–927 (2007). doi: 10.1038/nri2204; pmid: 17965637
42. F. Z. Chowdhury, L. D. Estrada, S. Murray, J. Forman, J. D. Farrar, Pharmacological inhibition of TPL2/MAP3K8 blocks human cytotoxic T lymphocyte effector functions. *PLOS ONE* **9**, e92187 (2014). doi: 10.1371/journal.pone.0092187; pmid: 24642963
43. W. Wei *et al*., Dual-specificity phosphatases 2: Surprising positive effect at the molecular level and a potential biomarker of diseases. *Genes Immun.* **14**, 1–6 (2013). doi: 10.1038/gene.2012.54; pmid: 23190643
44. R. M. Welsh, Blimp hovers over T cell immunity. *Immunity* **31**, 178–180 (2009). doi: 10.1016/j.immuni.2009.08.005; pmid: 19699168
45. L. C. Tsoi *et al*., Atopic Dermatitis Is an IL-13-Dominant Disease with Greater Molecular Heterogeneity Compared to Psoriasis. *J. Invest. Dermatol.* **139**, 1480–1489 (2019). doi: 10.1016/j.jid.2018.12.018; pmid: 30641038
46. A.-C. Villani *et al*., Single-cell RNA-seq reveals new types of human blood dendritic cells, monocytes, and progenitors. *Science* **356**, aah4573 (2017). doi: 10.1126/science.aah4573; pmid: 28428369
47. G. Hoeffel *et al*., Adult Langerhans cells derive predominantly from embryonic fetal liver monocytes with a minor contribution of yolk sac-derived macrophages. *J. Exp. Med.* **209**, 1167–1181 (2012). doi: 10.1084/jem.20120340; pmid: 22565823
48. M. P. Collin *et al*., The fate of human Langerhans cells in hematopoietic stem cell transplantation. *J. Exp. Med.* **203**, 27–33 (2006). doi: 10.1084/jem.20051787; pmid: 16390938
49. L. Ardouin *et al*., Broad and Largely Concordant Molecular Changes Characterize Tolerogenic and Immunogenic Dendritic Cell Maturation in Thymus and Periphery. *Immunity* **45**, 305–318 (2016). doi: 10.1016/j.immuni.2016.07.019; pmid: 27533013
50. B. Maier *et al*., A conserved dendritic-cell regulatory program limits antitumour immunity. *Nature* **580**, 257–262 (2020). doi: 10.1038/s41586-020-2134-y; pmid: 32269339
51. M. Baratin *et al*., T Cell Zone Resident Macrophages Silently Dispose of Apoptotic Cells in the Lymph Node. *Immunity* **47**, 349–362.e5 (2017). doi: 10.1016/j.immuni.2017.07.019; pmid: 28801233
52. S. Tamoutounour *et al*., Origins and functional specialization of macrophages and of conventional and monocyte-derived dendritic cells in mouse skin. *Immunity* **39**, 925–938 (2013). doi: 10.1016/j.immuni.2013.10.004; pmid: 24184057
53. T.-P. Vu Manh, N. Bertho, A. Hosmalin, I. Schwartz-Cornil, M. Dalod, Investigating Evolutionary Conservation of Dendritic Cell Subset Identity and Functions. *Front. Immunol.* **6**, 260 (2015). doi: 10.3389/fimmu.2015.00260; pmid: 26082777
54. T.-L. Tang-Huau *et al*., Human in vivo-generated monocyte-derived dendritic cells and macrophages cross-present antigens through a vacuolar pathway. *Nat. Commun.* **9**, 2570 (2018). doi: 10.1038/s41467-018-04985-0; pmid: 29967419
55. J.-E. Park *et al*., A cell atlas of human thymic development defines T cell repertoire formation. *Science* **367**, eaay3224 (2020). doi: 10.1126/science.aay3224; pmid: 32079746
56. T. A. Wynn, A. Chawla, J. W. Pollard, Macrophage biology in development, homeostasis and disease. *Nature* **496**, 445–455 (2013). doi: 10.1038/nature12034; pmid: 23619691
57. L. Chorro *et al*., Langerhans cell (LC) proliferation mediates neonatal development, homeostasis, and inflammation-associated expansion of the epidermal LC network. *J. Exp. Med.* **206**, 3089–3100 (2009). doi: 10.1084/jem.20091586; pmid: 19995948
58. D. Terhorst *et al*., Dynamics and Transcriptomics of Skin Dendritic Cells and Macrophages in an Imiquimod-Induced, Biphasic Mouse Model of Psoriasis. *J. Immunol.* **195**, 4953–4961 (2015). doi: 10.4049/jimmunol.1500551; pmid: 26466959
59. K. M. Bertram *et al*., Identification of HIV transmitting CD11c^{+} human epidermal dendritic cells. *Nat. Commun.* **10**, 2759 (2019). doi: 10.1038/s41467-019-10697-w; pmid: 31227717
60. J. B. Cheng *et al*., Transcriptional Programming of Normal and Inflamed Human Epidermis at Single-Cell Resolution. *Cell Rep.* **25**, 871–883 (2018). doi: 10.1016/j.celrep.2018.09.006; pmid: 30355494
61. M. B. Omary, N.-O. Ku, P. Strnad, S. Hanada, Toward unraveling the complexity of simple epithelial keratins in human disease. *J. Clin. Invest.* **119**, 1794–1805 (2009). doi: 10.1172/JCI37762; pmid: 19587454
62. A. Mishra *et al*., A protein phosphatase network controls the temporal and spatial dynamics of differentiation commitment in human epidermis. *eLife* **6**, e27356 (2017). doi: 10.7554/eLife.27356; pmid: 29043977
63. K. R. Feingold, Lamellar bodies: The key to cutaneous barrier function. *J. Invest. Dermatol.* **132**, 1951–1953 (2012). doi: 10.1038/jid.2012.177; pmid: 22797297
64. C. Trapnell *et al*., The dynamics and regulators of cell fate decisions are revealed by pseudotemporal ordering of single cells. *Nat. Biotechnol.* **32**, 381–386 (2014). doi: 10.1038/nbt.2859; pmid: 24658644
65. S. Joost *et al*., Single-Cell Transcriptomics Reveals that Differentiation and Spatial Signatures Shape Epidermal and Hair Follicle Heterogeneity. *Cell Syst.* **3**, 221–237.e9 (2016). doi: 10.1016/j.cels.2016.08.010; pmid: 27641957
66. S.-C. Lee *et al*., Expression of differentiation markers during fetal skin development in humans: Immunohistochemical studies on the precursor proteins forming the cornified cell envelope. *J. Invest. Dermatol.* **112**, 882–886 (1999). doi: 10.1046/j.1523-1747.1999.00602.x; pmid: 10383733
67. M. Seidl-Philipp *et al*., Spectrum of ichthyoses in an Austrian ichthyosis cohort from 2004 to 2017. *J. Dtsch. Dermatol. Ges.* **18**, 17–25 (2020). doi: 10.1111/ddg.13968; pmid: 31642606
68. H. B. Schonthaler *et al*., S100A8-S100A9 protein complex mediates psoriasis by regulating the expression of complement factor C3. *Immunity* **39**, 1171–1181 (2013). doi: 10.1016/j.immuni.2013.11.011; pmid: 24332034
69. U. Sivaprasad *et al*., SERPINB3/B4 contributes to early inflammation and barrier dysfunction in an experimental murine model of atopic dermatitis. *J. Invest. Dermatol.* **135**, 160–169 (2015). doi: 10.1038/jid.2014.353; pmid: 25111616
70. E. G. Harper *et al*., Th17 cytokines stimulate CCL20 expression in keratinocytes in vitro and in vivo: Implications for psoriasis pathogenesis. *J. Invest. Dermatol.* **129**, 2175–2183 (2009). doi: 10.1038/jid.2009.65; pmid: 19295614
71. H. He *et al*., Single-cell transcriptome analysis of human skin identifies novel fibroblast subpopulation and enrichment of immune subsets in atopic dermatitis. *J. Allergy Clin. Immunol.* **145**, 1615–1628 (2020). doi: 10.1016/j.jaci.2020.01.042; pmid: 32035984
72. T. Tammela, K. Alitalo, Lymphangiogenesis: Molecular mechanisms and future promise. *Cell* **140**, 460–476 (2010). doi: 10.1016/j.cell.2010.01.045; pmid: 20178740
73. J. Goveia *et al*., An Integrated Gene Expression Landscape Profiling Approach to Identify Lung Tumor Endothelial Cell Heterogeneity and Angiogenic Candidates. *Cancer Cell* **37**, 421 (2020). doi: 10.1016/j.ccell.2020.03.002; pmid: 32183954
74. A. Thiriot *et al*., Differential DARC/ACKR1 expression distinguishes venular from non-venular endothelial cells in murine tissues. *BMC Biol.* **15**, 45 (2017). doi: 10.1186/s12915-017-0381-7; pmid: 28526034
75. J. Pollheimer *et al*., Interleukin-33 drives a proinflammatory endothelial activation that selectively targets nonquiescent

cells. *Arterioscler. Thromb. Vasc. Biol.* **33**, e47–e55 (2013). doi: 10.1161/ATVBAHA.112.253427; pmid: 23162017
76. K. Veerman, C. Tardiveau, F. Martins, J. Coudert, J.-P. Girard, Single-Cell Analysis Reveals Heterogeneity of High Endothelial Venules and Different Regulation of Genes Controlling Lymphocyte Entry to Lymph Nodes. *Cell Rep.* **26**, 3116–3131.e5 (2019). doi: 10.1016/j.celrep.2019.02.042; pmid: 30865898
77. H. S. Phillips *et al*., Molecular subclasses of high-grade glioma predict prognosis, delineate a pattern of disease progression, and resemble stages in neurogenesis. *Cancer Cell* **9**, 157–173 (2006). doi: 10.1016/j.ccr.2006.02.019; pmid: 16530701
78. M. Barnat *et al*., Huntington's disease alters human neurodevelopment. *Science* **369**, 787–793 (2020). doi: 10.1126/science.aax3338; pmid: 32675289
79. Zenodo doi:10.5281/zenodo.4249674.

ACKNOWLEDGMENTS

We thank the Newcastle University Flow Cytometry Core Facility, Bioimaging Core Facility, Genomics Core Facility, and NUIT for technical assistance; the School of Computing for access to the High-Performance Computing Cluster; the Newcastle Molecular Pathology Node Proximity Lab and A. Farnworth for clinical liaison; and the Newcastle Dermatology Department for critical feedback. The human embryonic and fetal material was provided by the Joint MRC/Wellcome (MR/R006237/1) Human Developmental Biology Resource (www.hdbr.org). We thank F. Kreeshan and W. Ghumra for their help with the methotrexate study in AD and collection of samples. We thank J. Elias (scientific illustrator) for her support with the print page summary figure design. This publication is part of the Human Cell Atlas, www.humancellatlas.org/publications. **Funding:** We acknowledge funding from the Wellcome Human Cell Atlas Strategic Science Support (WT211276/Z/18/Z); M.H. is funded by Wellcome (WT107931/Z/15/Z), the Lister Institute for Preventive Medicine and Newcastle NIHR Biomedical Research Centre (BRC); S.A.T. is funded by Wellcome (WT206194), ERC Consolidator and EU MRG-Grammar awards; N.J.R. is a NIHR Senior Investigator funded by Newcastle NIHR BRC, Newcastle MRC/EPSRC Molecular Pathology Node, and Newcastle NIHR Medtech Diagnostic Co-operative, and has received research grant funding from Novartis, PSORT partners (www.PSORT.org.uk), and income to Newcastle University from Almirall, Lily, and Novartis for attendance at advisory boards; F.M.W. gratefully acknowledges financial support from the Medical Research Council (MR/PO18823/1), the Wellcome Trust (096540/Z/11/Z), and the Department of Health via the National Institute for Health Research comprehensive Biomedical Research Centre (BRC) award to Guy's & St Thomas' National Health Service Foundation Trust in partnership with King's College London and King's College Hospital NHS Foundation Trust; E.A.O. has received research funding from Kamari Pharma in the current fiscal year and has been on a grants advisory board for Sanofi-Aventis (money to University); E.F.M.P. is funded by a Wellcome 4ward-North Clinical Training Fellowship; G.S.O. receives funding from the Medical Research Council UK, NIHR Oxford Biomedical Research Centre, Wellcome Trust, and NIHR Clinical Research Network administered through the Radcliffe Department of Medicine, University of Oxford; and P.H.J. is supported by Wellcome Trust grant 296194 and Cancer Research UK Programme Grant C609/A27326. **Author contributions:** M.H., F.M.W., and S.A.T. conceived and co-directed the study; M.H., S.A.T., F.M.W., J.F., E.F.M.P., A.-C.V., N.J.R., and G.R. designed the experiments; samples were isolated by J.F., R.A.B., and E.F.M.P.; libraries were prepared by E.S., J.E., and J.C.; flow cytometry and CyTOF experiments were designed and performed by J.F., G.R., D.M., D.McD., E.F.M.P., A.F., and R.A.B.; immunohistochemistry and immunofluorescence were performed by D.D., E.F.M.P., C.J., T.N., and C.C.; P.V., G.R., I.G., N.H., J.F., K.G., M.E., D.-M.P., and K.P. performed the computational analysis; M.H., J.F., P.V., G.R., R.A.B., E.F.M.P., E.S., A.D., F.M.W., S.A.T., G.S.O., E.A.O., N.J.R., N.R., P.H.J., M.E., T.H., J.-E.P., B.S., A.-C.V., S.W., J.B., R.V.-T., S.B., D.McD., A.F., X.W., L.J., K.B.M., D.B., B.O., M.D.L., A.H., and S.L. interpreted the data; and M.H., G.R., J.F., P.V., E.F.M.P., E.S., B.O., A.D., F.M.W., and S.A.T. wrote the manuscript. All authors read and accepted the manuscript. **Competing interests:** F.M.W. is on secondment as Executive Chair of the UK Medical Research Council. In the past 3 years, S.A.T. has been remunerated for consulting by Genentech and Roche, and is a member of the scientific advisory boards of GlaxoSmithKline, Biogen, and Foresite Labs. **Data and materials availability:** The raw sequencing data and expression count data with cell classifications are deposited at ArrayExpress: www.ebi.ac.uk/arrayexpress/experiments/E-MTAB-8142. All data analysis scripts are available on Zenodo DOI: 10.5281/zenodo.4249674 (*79*).

SUPPLEMENTARY MATERIALS

science.sciencemag.org/content/371/6527/eaba6500/suppl/DC1
Materials and Methods
Figs. S1 to S7
Tables S1 to S6
References (*80*–*89*)

21 December 2019; resubmitted 3 September 2020
Accepted 1 December 2020
10.1126/science.aba6500